



A Journal of the Gesellschaft Deutscher Chemiker

Angewandte Chemie

GDCh

International Edition

www.angewandte.org

Accepted Article

Title: Rational Manipulation of Stacking Arrangements in Three-Dimensional Zeolites Built from Two-Dimensional Zeolitic Nanosheets

Authors: Le Xu, Tianqiong Ma, Yihan Shen, Yong Wang, Lu Han, Watcharop Chaittisilp, Toshiyuki Yokoi, Junliang Sun, Toru Wakihara, and Tatsuya Okubo

This manuscript has been accepted after peer review and appears as an Accepted Article online prior to editing, proofing, and formal publication of the final Version of Record (VoR). This work is currently citable by using the Digital Object Identifier (DOI) given below. The VoR will be published online in Early View as soon as possible and may be different to this Accepted Article as a result of editing. Readers should obtain the VoR from the journal website shown below when it is published to ensure accuracy of information. The authors are responsible for the content of this Accepted Article.

To be cited as: *Angew. Chem. Int. Ed.* 10.1002/anie.202009336

Link to VoR: <https://doi.org/10.1002/anie.202009336>

Rational Manipulation of Stacking Arrangements in Three-Dimensional Zeolites Built from Two-Dimensional Zeolitic Nanosheets

Le Xu, Tianqiong Ma, Yihan Shen, Yong Wang, Lu Han*, Watcharop Chaitsisilp, Toshiyuki Yokoi, Junliang Sun*, Toru Wakihara, and Tatsuya Okubo*

Abstract: Unit-cell-thin zeolitic nanosheets have emerged as fascinating materials for catalysis and separation. The controllability of nanosheets stacking is extremely challenging in the chemistry of two-dimensional zeolitic materials. So far, the organization of zeolitic nanosheets in hydrothermal synthesis has been limited by the lack of tunable control over the guest-host interactions between organic structure-directing agents (OSDAs) and zeolitic nanosheets. Here, we report a direct synthetic methodology that enables systematic manipulation of the aluminosilicate MWW-type nanosheets stacking. Variable control of guest-host interactions is rationally achieved by synergistically altering the charge density of OSDAs and synthetic silica-to-alumina composition. These finely-controlled interactions allow the successful preparation of series of three-dimensional (3D) zeolites with MWW-layer stacking in wide ranges from variations of disorder to fully-order, leading to tunable catalytic activity in cracking reaction. These results highlight unprecedented opportunities to modulate zeolitic nanosheets arrangement in 3D zeolites whose structure can be tailored for catalysis and separation.

Zeolites, a class of crystalline microporous materials, have been widely utilized as solid acid catalysts in the conversion of petroleum-derived hydrocarbons to valuable chemical products.^[1] As a sub-family of zeolitic materials, two-dimensional (2D) lamellar zeolites have gained much attention as promising materials in catalysis and separation fields due to the unit-cell-thin nanosheet thickness and flexible stacking feature.^[2] In fundamental zeolite chemistry, zeolitic nanosheets provide a unique platform to construct zeolites by linking 2D building blocks in different patterns.^[3] Various stacking modes and linkages between zeolitic nanosheets have expanded the types of zeolite structures with different pore entrances,^[4] which intimately determine its size/shape selectivity in applications. In this respect, the control of nanosheets stacking is of paramount significance for constructing targeted zeolites with tailored porosity and function. Although postsynthetic approaches have been developed to regulate nanosheets stacking,^[5] they often lack of precise control over the

treatment processes. In hydrothermal synthesis, the formation and organization of zeolitic nanosheets is controlled by the guest-host interactions between OSDA and zeolitic nanosheets. A suitable OSDA with strong interaction with a specific Miller plane of zeolite structure would inhibit crystal growth along one crystallographic dimension, leading to the formation of 2D zeolitic nanosheets stacking in energetic favorable modes.^[6] However, owing to the lack of understanding of zeolite crystallization and poor control of guest-host interactions, rational design of a synthetic method for finely controlling nanosheets stacking remains a fundamental challenge.

Herein, we reported the systematic and tunable manipulation of the typical MWW-layer stacking through controllable guest-host interactions between OSDAs and 2D zeolitic nanosheets. Conceptually, this variable control was rationally realized by altering the charge density of OSDA and synthetic silica-to-alumina composition. First, our synthesis utilized three related OSDAs containing the same imidazolium moiety but with different alkylated groups, which are isobutyl, cyclohexyl and cycloheptyl, resulting in three OSDAs, namely 1,3-bis(isobutyl) imidazolium (C₄-IM), 1,3-bis(cyclohexyl) imidazolium (C₆-IM) and 1,3-bis(cycloheptyl) imidazolium (C₇-IM), respectively (Figs. 1a, 1c and 1e). The key benefit of using these OSDAs is that the difference of substituents on the aromatic ring would influence the charge density in the resulting OSDAs, which can be demonstrated by density functional theory (DFT) calculations. The calculated electrostatic potential (ESP) mapping showed a significant difference in the ESP surface (i.e., charge density) among three OSDAs, as the ESP of OSDA gradually decreased with the increasing size of substituents (ESP: C₄-IM > C₆-IM > C₇-IM, Figs. 1b, 1d and 1f). Although three OSDAs had the same total positive charge of +1, C₄-IM exhibited the highest positive charge density, which gradually decreased in C₆-IM and

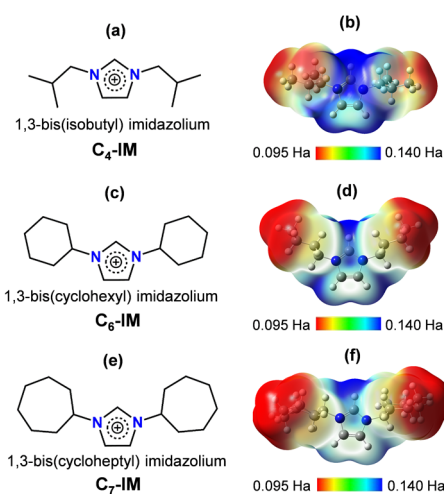


Figure 1. Three related OSDAs that used for zeolite synthesis in this work. (a) 1,3-bis(isobutyl) imidazolium (C₄-IM), (c) 1,3-bis(cyclohexyl) imidazolium (C₆-IM) and (e) 1,3-bis(cycloheptyl) imidazolium (C₇-IM). The electrostatic potentials (ESP) mapped onto their electron density surface were given to (b) C₄-IM, (d) C₆-IM and (f) C₇-IM, respectively. The positive charge density of three OSDAs gradually decreased with the increasing size of alkylated groups on the imidazolium ring, as demonstrated by the decreasing ESP energy in the order of C₄-IM, C₆-IM and C₇-IM.

[*] Dr. L. Xu, Prof. T. Wakihara, Prof. T. Okubo
Department of Chemical System Engineering, The University of Tokyo
Tokyo 113-8656, Japan
E-mail: okubo@chemsys.t.u-tokyo.ac.jp

Dr. T. Ma, Y. Shen, Prof. J. Sun
College of Chemistry and Molecular Engineering, Peking University
Beijing 100871, China
E-mail: junliang.sun@pku.edu.cn

Prof. L. Han
School of Chemical Science and Engineering, Tongji University
Shanghai 200092, China
E-mail: luhan@tongji.edu.cn

Dr. Y. Wang, Prof. T. Yokoi,
Chemical Resources Laboratory, Tokyo Institute of Technology
Yokohama 226-8503, Japan

Prof. W. Chaikittisilp
Research and Services Division of Materials Data and Integrated System
National Institute for Materials Sciences (NIMS)
Ibaraki 305-0044, Japan

Supporting information for this article is given via a link at the end of the document.

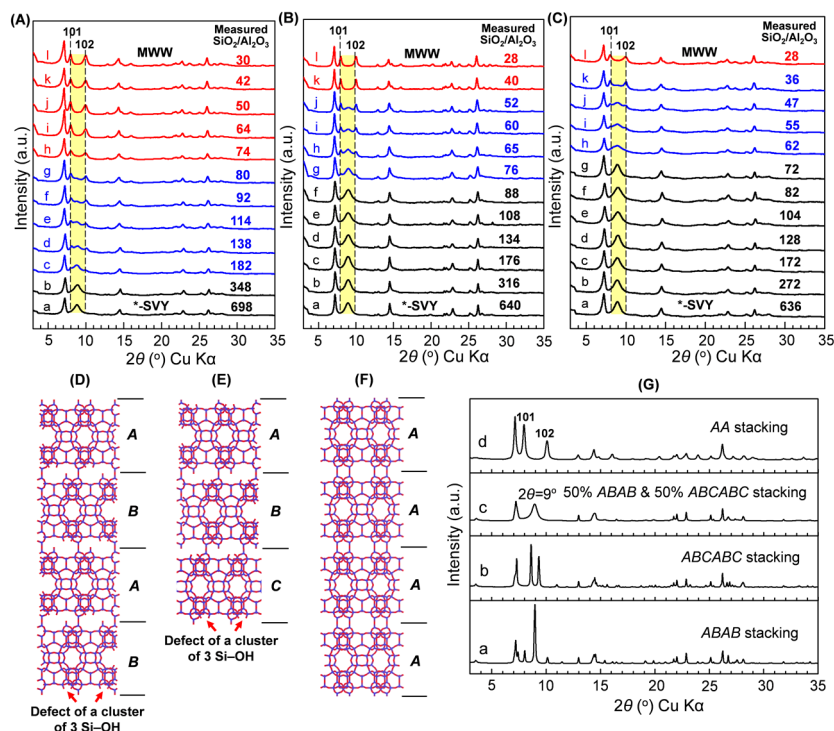


Figure 2. XRD patterns of zeolites that synthesized using (A) C_4 -IM, (B) C_6 -IM, and (C) C_7 -IM as OSDA and with different synthetic $\text{SiO}_2/\text{Al}_2\text{O}_3$ ratios (SAR) in gels: (a) 800, (b) 400, (c) 200, (d) 150, (e) 120, (f) 100, (g) 90, (h) 80, (i) 70, (j) 60, (k) 50 and (l) 40. The structure models of (D) shifted ABAB, (E) shifted ABCABC and (F) ordered AA MWW-layer stacking. (G) The simulated XRD patterns of (a) ABAB stacking, (b) ABCABC stacking, (c) 50% ABAB and 50% ABCABC stacking and (d) AA stacking. The experimental XRD patterns plotted in black in (A–C) indicated the faulted structure containing two shifted stacking modes. The XRD patterns in blue indicated the structure transformation due to the MWW-layer stacking change from disorder to order. The XRD patterns in red represented the ordered MWW-layer stacking in the AA mode. The main differences of XRD patterns among different materials were highlighted in yellow regions. The two shifted structures (D and E) were found to intergrow to form a disordered stacking with nearly 50% ABAB and 50% ABCABC mode, leading to a broad XRD peak at 2θ of 9° (Gc). The typical MWW topology contained the ordered AA MWW-layer stacking, resulting in two well-resolved 101 and 102 XRD peaks (Gd).

C_7 -IM, respectively. Therefore, it was clear that the charge density of OSDA could be adjusted according to the size of alkylated groups on the imidazolium ring.

With three related OSDAs, the systematic variations of a single variable (OSDA-type) in zeolite synthesis could be achieved at a specific silica-to-alumina ratio ($\text{SiO}_2/\text{Al}_2\text{O}_3$, SAR) in synthetic gel. Moreover, for each OSDA, the synthetic SAR composition was varied in a wide range of 800–40 to investigate the structure-directing behavior of OSDAs under different synthetic SAR conditions. First, 2D MWW layered precursors were obtained for each OSDA in all synthetic SAR ranges, as evidenced by the typical change in their X-ray diffraction (XRD) patterns of as-synthesized samples during calcination (Figs. S1–S3).^[3a,7] For the synthesis with a high synthetic SAR of 800, the zeolites with similar highly-disordered structure were produced with each OSDA (Figs. 2Aa, 2Ba and 2Ca), which was consistent with previous reports that these OSDAs directed the SSZ-70 zeolite (*-SVY topology) containing disordered MWW-layer stacking (Figs. 2D, 2E and 2Gc).^[8] However, an unexpected transition of MWW-layer stacking from disorder to order was observed when the synthetic SAR decreased, regardless of OSDA-types (Figs. 2A–2C and Figs. S1–S3). The intensity of the broad XRD reflection centered at 2θ of 9° in the XRD pattern, representing the disordered MWW-layer stacking,^[9] gradually decreased with the decreasing synthetic SAR, and eventually disappeared at a low synthetic SAR. Meanwhile, the new 101 and 102 reflections, typical for the ordered MWW-layer stacking (Fig. 2Gd),^[3a,7b] started to appear with the decreasing synthetic SAR (Figs.

2A–2C). Therefore, our findings indicated these OSDAs not only played the role of structure-direction for the MWW-type layered structure, but also acted as a modulator to regulate zeolitic nanosheets stacking in different SAR ranges. As is well-known that OSDAs have been extensively employed in zeolite synthesis with the aims to search for new structure,^[10] regulate crystallite morphology and size,^[11] alternate framework composition^[12] and control of aluminum location and proximity,^[13] however, this modulation effect of OSDA on zeolitic layer stacking has never been discovered to the best of our knowledge.

More interestingly, different synthetic SAR ranges for stacking transition were observed for different OSDAs. The transition from disordered to ordered nanosheet stacking occurred in the highest synthetic SAR range of 200–90 for C_4 -IM (Figs. 2Ac–2Ag), while the lowest synthetic SAR range of 80–50 was observed for C_7 -IM (Figs. 2Ch–2Ck). With C_6 -IM as OSDA, the medium synthetic SAR range (90–60) worked for stacking transition (Figs. 2Bg–2Bj). Elemental analysis confirmed the above tendency that OSDA with a smaller substituent produced zeolites with a higher SAR range for stacking transition (Tables S1–S3). Besides, trace amounts of Na^+ were found in the as-synthesized zeolites within the structure transition range, while the OSDA contents were much higher by comparison (Fig. S4). This indicated OSDA played a much more important role in governing MWW-layers stacking compared with trace amount of Na^+ .

²⁷Al MAS NMR spectra of as-synthesized products with C_6 -IM as OSDA indicated Al species were incorporated into the tetrahedral sites in MWW-layer (Fig. S5). Since the substitution of anionic $\text{AlO}_4/2^-$ for framework $\text{SiO}_4/2^-$ tetrahedral units would introduce the anionic lattice charges, cationic OSDA was generally needed in the high-silica zeolite synthesis to provide the electrostatic compensation for anionic lattice charges.^[14] For layered zeolite synthesis, the influence of guest-host interactions on nanosheet stacking would become much more significant when related OSDAs had similar structure-directing ability but possessed different charge densities. The mismatch between the charge density of OSDA and synthetic SAR seems to provide the driving force to move MWW nanosheets. With the highest positive charge density, C_4 -IM would interact with less negatively-charged anionic zeolite lattice (i.e. high framework SARs) at their interface much stronger than C_6 -IM and C_7 -IM, probably providing more stabilization energy to overcome the energetic barrier for nanosheet stacking mode transition. Thus, the stacking transition was observed among zeolites with high SARs ranging from 182 to 80 for C_4 -IM (Figs. 2Ac–2Ag, and Table S1). In contrast, C_7 -IM with the lowest positive charge density would interact with zeolite lattice strong enough to induce nanosheet stacking transition, only when zeolite lattice had low SARs of 62–36 and thus became much more negatively-charged (Figs. 2Ch–2Ck and Table S3).

Although the mechanism of zeolite crystallization has not been well-clarified, it was reasonable to speculate the guest-host interactions between OSDAs and anionic zeolitic lattice during crystallization could be adjusted according to the charge density of OSDAs and synthetic SAR composition. For each OSDA, the

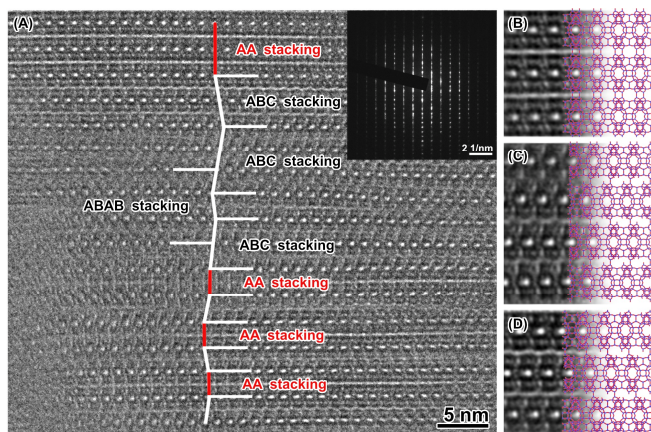


Figure 3. (A) TEM image and corresponding SAED pattern of the zeolite MWW-C₆-SAR60, which was synthesized with C₆-IM as OSDA and had a SAR of 60 (determined by ICP-AES analysis). (B–D) The Fourier filtered TEM images with AA, ABAB and ABCABC stacking sequences, respectively

tunable control of the guest-host interactions was realized by altering the synthetic SAR compositions. For the synthesis with a specific synthetic SAR, the variable control was achieved by using different OSDAs. Thus, a great advantage of our synthetic approach is that the cooperation of three relevant OSDAs and various synthetic SAR compositions allowed the preparation of three zeolite families with well-controlled MWW-layer stacking modes in wide ranges from variations of highly-disorder to fully-order, which has not been achieved in previous studies.

To investigate the stacking structure of MWW-layer in the resulting material, zeolite MWW-C₆-SAR60 that synthesized with C₆-IM as OSDA and had a SAR of 60 was used for transmission electron microscopy (TEM) investigations. The selected-area electron diffraction (SAED) pattern showed sharp diffraction spots for reflections with indices $h = 3n$ while streaks for reflections with $h = 3n \pm 1$, indicating the shift of layers along $\pm 1/3a^*$ (a^* denotes the reciprocal space vector). The organization of MWW layers with various stacking sequences could be identified from the high resolution TEM (HRTEM) image, which clearly showed the material contained the stacking of MWW-layers in not only the ordered AA sequence but also the shifted ABAB and ABCABC stacking modes (Fig. 3). It is worthy to note that this is the first time to directly observe a zeolite material that constructed with three different stacking modes of MWW-layer. Moreover, focusing on zeolites prepared with C₆-IM as OSDA in the wide SAR range of 640–28 (Figs. 2Ba–2Bi), XRD simulation by the Discry program^[15] indicated that the content of AA stacking was negligible in the high SAR range (640–88), but gradually enhanced during structure transition (SAR of 76–52), and finally became the main phase in the low SAR range of 40–28 (Fig. S6). Meanwhile, the contents of shifted structures (ABAB and ABCABC) gradually decreased with the increasing content of AA stacking mode.

With the advantage of well-controlled zeolitic MWW-layer stacking, our synthetic method offered an unprecedented opportunity to prepare zeolites with comparable SAR compositions but in different stacking modes. The most interesting examples were three different zeolites with a closed measured SAR around 60 could be synthesized with three different OSDAs. In particular, C₄-IM directed MWW-C₄-SAR64 zeolite with the highly-ordered MWW-layer stacking (Figs. 2Ai and 4Aa), while the partially-disordered MWW-C₆-SAR60 zeolite (Figs. 2Bi and 4Ab) and the highly-disordered MWW-C₇-SAR62 zeolite (Figs. 2Ch and 4Ac) were prepared with C₆-IM and C₇-IM, respectively. XRD simulation revealed that they

possessed different contents of stacking modes (Fig. S7). Based on these three zeolites, it would be interesting to explore the influence of stacking structures on the property and function of zeolite.

Scanning electron microscopy (SEM) images of three zeolites showed the typical flask-like crystal morphology and similar crystal dimension (Fig. S8). ¹³C MAS NMR spectra demonstrated three OSDAs kept intact in the as-synthesized layered precursors (Fig. S9). Although ²⁷Al MAS NMR spectra of as-synthesized materials indicated Al species were incorporated into MWW-layers (Fig. S10), it was interesting to observe less dealumination in the calcined-form MWW-C₆-SAR60 and MWW-C₇-SAR62 zeolites (Figs. 4Bb and 4Bc). We postulated that the different dealumination degrees might be, at least partially, related to the MWW-layer stacking. Previous NMR investigation has shown that C₄-IM directed 94% of framework Al atoms sited near the MWW-layer surface.^[16] According to the MWW-layer structure, T1 site was one possible position to hold the surface Al atoms (Fig. S11). Since there was no T1–O–T1 linkage in the as-synthesized precursors, Al atoms were allowed to simultaneously distribute at T1 sites on both sides of adjacent MWW-layers. However, the interlayer condensation would lead to the formation of bridged T1–O–T1 bonds between layers. Owing to the Löwenstein's rule,^[17] some Al species would force to remove out of zeolite framework during calcination, when both paired T1 sites on neighboring layers were occupied by Al atoms. For MWW-C₄-SAR64, calcination led to the condensation between each pair of T1–OH (Fig. S11a), rising more chances to generate the energetically unfavorable Al–O–Al linkages. With less contents of ordered stacking in MWW-C₆-SAR60 and MWW-C₇-SAR62 (Fig. S7), less T1–O–T1 bridges would be generated during calcination (Fig. S11b), probably leading to less chance to produce extra-framework Al (EF-Al) species. Thus, the adjustable manipulation of MWW-layer stacking might endow MWW-C₆-SAR60 and MWW-C₇-SAR62 resistance to dealumination during calcination.

In addition to dealumination, the stacking control of zeolitic nanosheets also affected the intracrystalline defects and acid strengths of the resulting materials. IR spectra of the acid form of three zeolites exhibited the vibrations corresponding to bridged hydroxyl groups at 3620 cm⁻¹ and external silanol at 3744 cm⁻¹ (Fig. S12). A shoulder at 3728 cm⁻¹ assigned to the intracrystalline silanols was also observed, and its intensity increased with the increasing content of disordered stacking structure. A previous study demonstrated the disordered MWW zeolite material contained two kinds of silanols on the layer surface, namely the single terminal Si–OH and a cluster of 3 Si–OH (Fig. S13).^[9a,18] Thus, the presence of more intracrystalline defects in MWW-C₆-SAR60 and MWW-C₇-SAR62 was consistent with the high contents of disordered stacking structure in these two materials (Fig. S7). The highly-ordered MWW-C₄-SAR64 had less intracrystalline defects, which have also been observed in MCM-22.^[19] Moreover, pyridine was readily adsorbed at room temperature on dehydrated samples (Figs. 4Da, 4Ea and 4Fa). However, a large amount of protonated pyridine was still retained on MWW-C₄-SAR64 after desorption at 450 °C (Fig. 4Dd and Table S4), indicating the higher amount of strong acid sites, as compared with MWW-C₆-SAR60 and MWW-C₇-SAR62 that showed gradually decreased amount of strong acid sites, especially the Brønsted acid sites (Figs. 4E, 4F and Table S4). This observation was further confirmed by NH₃-TPD results of three controlled materials (Fig. 4C).

With the highly-ordered stacking, MWW-C₄-SAR64 exhibited a higher specific surface area and a larger micropore volume, compared with other two materials (Fig. S14 and Table S5). However, the partially-disordered MWW-C₆-SAR60 zeolite and

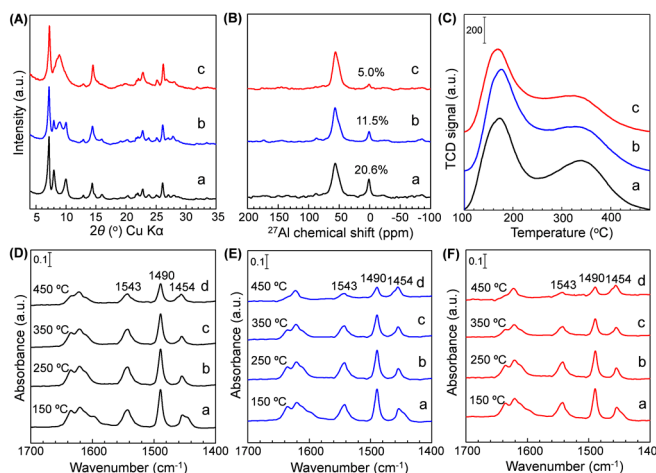


Figure 4. (A) XRD patterns, (B) solid-state ^{27}Al MAS NMR spectra and (C) NH_3 -TPD of the proton-type calcined zeolite products: (a) MWW- C_4 -SAR64, (b) MWW- C_6 -SAR60 and (c) MWW- C_7 -SAR62. Pyridine-adsorption FTIR spectra of proton-type calcined zeolite products: (D) MWW- C_4 -SAR64, (E) MWW- C_6 -SAR60 and (F) MWW- C_7 -SAR62 after desorption at (a) 150 °C, (b) 250 °C, (c) 350 °C and (d) 450 °C, respectively. In (D–F), the 1543 cm^{-1} and 1454 cm^{-1} peak represented the pyridine-bonded Brønsted and Lewis acidic sites, respectively.

highly-disordered MWW- C_7 -SAR62 zeolite showed lower but similar specific surface area and micropore volume, which could be caused by the combined effects of structure and dealumination. Although a higher content of the ordered AA stacking in MWW- C_6 -SAR60 (compared with MWW- C_7 -SAR62, Fig. S7) would lead to a relative higher N_2 adsorption capacity (Fig. S15), more serious dealumination led to partial micropore-blockage in MWW- C_6 -SAR60 (Fig. 4Bb). In contrast, the dealumination-related micropore blockage was less significant for MWW- C_7 -SAR62 because of less EF-Al species (Fig. 4Bc). This combined effects resulted in the comparable specific surface area and micropore volume between MWW- C_6 -SAR60 and MWW- C_7 -SAR62.

Therefore, three OSDAs regulated the stacking of MWW-layer in three resulting materials, which exhibited well-tuned properties in many aspects, such as dealumination, intracrystalline defect, acid strength and microporosity, among which the highly-ordered MWW- C_4 -SAR64 zeolite exhibited higher specific surface area, larger micropore volume and higher amount of strong acid sites. Besides, although the partially-disordered MWW- C_6 -SAR60 and highly-disordered MWW- C_7 -SAR62 zeolites had the lower but comparable microporosity, they exhibited different acid strengths. MWW- C_6 -SAR60 zeolite had the medium acidity, while MWW- C_7 -SAR62 only possessed a weak acidity. The catalytic cracking of *n*-hexane was used as a model reaction to investigate their catalytic behaviors. Compared with other two materials, MWW- C_4 -SAR64 led to a higher conversion of *n*-hexane and higher selectivity for the ethylene and propylene (Figs. S16 and S17), probably due to the benefit of larger specific surface area and strong acid strength. A lower but comparable hexane conversion was observed for MWW- C_6 -SAR60 and MWW- C_7 -SAR62 zeolites, indicating the comparable amount of reactant hexane could diffuse into the two independent channel systems and interact with acidic active sites in these two materials. For partially disordered and highly disordered zeolites, owing to the medium strong acidity of MWW- C_6 -SAR60 zeolite, relatively more propylene was produced. However, MWW- C_7 -SAR62 zeolite with the weak acid strength produced less propylene but more butane and butene isomers. Overall, the porosity and acidity parameters can be finely tuned, as a result of different stacking modes in three catalysts, leading to the controlled catalytic performances.

In summary, we report a new synthetic system that for the first time realizes the systematic manipulation of zeolitic nanosheet stacking. Owing to the tunable charge density of OSDAs and synthetic SAR compositions, the adjustable guest-host interactions become possible, leading to three new zeolite families containing well-controlled MWW-layer stacking modes in a wide range of variations from disorder to fully-order manners. Our study reveals that a new role of OSDA during zeolite crystallization, in which the OSDA can not only play the role of structure-direction, but also act as a modulator to regulate the nanosheet stacking. Furthermore, the concept of this new approach opens us to the possibility that this modulation effect would not be restricted to the MWW-type aluminosilicate, but should be applicable to other layered zeolites in general. More than 15 known zeolite topologies can be prepared through 2D layered precursor containing various trivalent/divalent heteroatoms. Therefore, the significance of this new synthetic approach is offering the possibility to design well-controlled zeolitic nanosheet arrangements in 3D zeolites whose structural features can be tailored for applications in catalysis and separation.

Acknowledgement

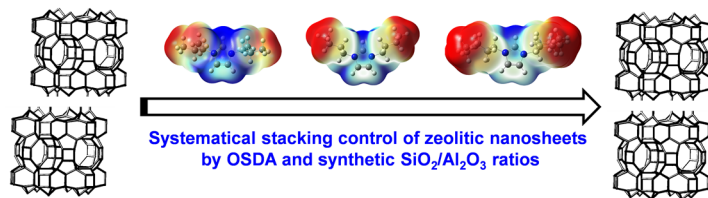
L.X. acknowledge Japan Society for the Promotion of Science (JSPS) for providing the research fellowship. L.H. and J.S. thanks the financial support from National Natural Science Foundation of China (L.H.: Grant nos. 21922304 and 21873072; J.S.: Grant no. 21871009) and Natural Science Foundation of Shanghai (L.H.: Grant no. 18ZR1442400).

Keywords: crystal growth • layered compounds • structure transformation • zeolites • catalysis

- [1] M. E. Davis, *Nature* **2002**, *417*, 813.
- [2] a) A. Corma, V. Fornes, S. B. Pergher, T. L. M. Maesen, J. G. Buglass, *Nature* **1998**, *396*, 353; b) K. Varoon, X. Zhang, B. Elyassi, D. D. Brewer, M. Gettel, S. Kumar, J. A. Lee, S. Maheshwari, A. Mittal, C. Sung, M. Cococcioni, L. F. Francis, A. V. McCormick, K. A. Mkhoyan, M. Tsapatsis, *Science* **2011**, *334*, 72; c) H. Luo, V. Michaelis, S. Hodges, R. Griffin, Y. Roman-Leshkov, *Chem. Sci.* **2015**, *6*, 6320; d) V. Margarit, M. Martinez-Armero, T. Navarro, C. Martinez, A. Corma, *Angew. Chem. Int. Ed.* **2015**, *54*, 13724; (e) L. Xu, X. Ji, S. Li, Z. Zhou, X. Du, J. Sun, F. Deng, S. Che, P. Wu, *Chem. Mater.* **2016**, *28*, 4512; f) Y. Zhou, Y. Mu, H. Hsieh, B. Kabius, C. Pacheco, C. Bator, R. M. Rioux, J. D. Rimer, *J. Am. Chem. Soc.* **2020**, *142*, 8211.
- [3] a) M. E. Leonowicz, J. A. Lawton, S. L. Lawton, M. K. Rubin, *Science* **1994**, *264*, 1910; b) W. J. Roth, P. Nachtigall, R. E. Morris, J. Čejka, *Chem. Rev.* **2014**, *114*, 4807; c) P. Eliasova, M. Opanasenko, P. S. Wheatley, M. Shamzhy, M. Mazur, P. Nachtigall, W. J. Roth, R. E. Morris, J. Čejka, *Chem. Soc. Rev.* **2015**, *44*, 7177; d) P. S. Wheatley, P. Chlubna-Eliášová, H. Greer, W. Zhou, V. R. Seymour, D. M. Dawson, S. E. Ashbrook, A. B. Pinar, L. B. McCusker, M. Opanasenko, J. Čejka, R. E. Morris, *Angew. Chem. Int. Ed.* **2014**, *53*, 13210.
- [4] B. Marler, Y. Wang, J. Song, H. Gies, *Dalton Trans.* **2014**, *43*, 10396.
- [5] a) T. Moteki, W. Chaikittsilp, A. Shimojima, T. Okubo, *J. Am. Chem. Soc.* **2008**, *130*, 15780; b) L. Xu, J. Sun, *Adv. Energy Mater.* **2016**, *6*, 1600441; c) L. Xu, P. Wu, *New J. Chem.* **2016**, *40*, 3958.
- [6] M. Witman, S. Ling, P. Boyd, S. Barthel, M. Haranczyk, B. Slater, B. Smit, *ACS Cent. Sci.* **2018**, *4*, 235.
- [7] a) M. K. Rubin, P. Chu, US Patent **1990**, 4954325; b) M. A. Cambor, A. Corma, M. Diaz-Cabanas, C. Baerlocher, *J. Phys. Chem. B* **1998**, *102*, 44.
- [8] a) R. H. Archer, J. R. Carpenter, S. Hwang, A. W. Burton, C. Chen, S. I. Zones, M. E. Davis, *Chem. Mater.* **2010**, *22*, 2563; b) R. H. Archer, S. I. Zones, M. E. Davis, *Microporous Mesoporous Mater.* **2010**, *130*, 255.
- [9] a) S. Smeets, Z. J. Berkson, D. Xie, S. I. Zones, W. Wan, X. Zou, M. Hsieh, B. F. Chmelka, L. B. McCusker, C. Baerlocher, *J. Am. Chem. Soc.* **2017**, *139*, 16803; b) L. Xu, X. Ji, J. Jiang, L. Han, S. Che, P. Wu, *Chem. Mater.* **2015**, *27*, 7852.
- [10] M. Moliner, F. Rey, A. Corma, *Angew. Chem. Int. Ed.* **2013**, *52*, 13880.

- [11] a) G. Bonilla, I. Diaz, M. Tsapatsis, H. Jeong, Y. Lee, D. G. Vlachos, *Chem. Mater.* **2004**, *16*, 5697; b) S. Mintova, J. P. Gilson, V. Valtchev, *Nanoscale* **2013**, *5*, 6693.
- [12] R. M. Barrer, P. J. Denny, *J. Chem. Soc.* **1961**, 971.
- [13] a) J. R. Di Iorio, C. T. Nimlos, R. Gounder, *ACS Catal.* **2017**, *7*, 6663; b) K. Muraoka, W. Chaikittsilp, Y. Yanaba, T. Yoshikawa, T. Okubo, *Angew. Chem. Int. Ed.* **2018**, *57*, 3742.
- [14] a) M. E. Davis, R. F. Lobo, *Chem. Mater.* **1992**, *4*, 756; b) Y. Li, H. Cao, J. Yu, *ACS Nano* **2018**, *12*, 4096; c) J. H. Lee, M. B. Park, J. K. Lee, H. Min, M. K. Song, S. B. Hong, *J. Am. Chem. Soc.* **2010**, *132*, 12971.
- [15] X. Wang, Y. Shen, R. Liu, X. Liu, C. Lin, D. Shi, Y. Chen, F. Liao, J. Lin, J. Sun, *Acta Cryst.* **2019**, *B75*, 333.
- [16] Z. J. Berkson, M. Hsieh, S. Smeets, D. Gajan, A. Lund, A. Lesage, D. Xie, S. I. Zones, L. B. McCusker, C. Baerlocher, B. F. Chmelka, *Angew. Chem. Int. Ed.* **2019**, *58*, 6255.
- [17] W. Löwenstein, *Am. Mineral.* **1954**, *39*, 92.
- [18] C. Schroeder, C. Muck-Lichtenfeld, L. Xu, N. A. Grosso-Giordano, A. Okrut, C. Chen, S. I. Zones, A. Katz, M. R. Hansen, H. Koller, *Angew. Chem. Int. Ed.* **2020**, *59*, 10939.
- [19] A. Corma, C. Corell, V. Fornes, W. Kolodzjski, J. Perez-Pariente, *Zeolites*, **1995**, *15*, 576.

COMMUNICATION



L. Xu, T. Ma, Y. Shen, Y. Wang, L. Han*,
W. Chaikittisilp, T. Yokoi, J. Sun*, T.
Wakihara, and T. Okubo*

Page No. – Page No.

**Rational Manipulation of Stacking
Arrangements in Three-Dimensional
Zeolites Built from Two-Dimensional
Zeolitic Nanosheets**

Stacking Modulation. A new synthetic method for the first time realizes the systematic manipulation of two-dimensional zeolitic nanosheets stacking in 3D zeolite, opening the possibilities of designing zeolitic nanosheet arrangements whose structure can be tailored for applications in catalysis and separation.